中國機械工程學刊第四十三卷第一期第 1~10 頁(民國一百一十一年)
Journal of the Chinese Society of Mechanical Engineers, Vol.43, No.1, pp 1~10 (2022)

Hypersonic Thermal Flow Past a Spherically Blunted Tangent-Ogive Nose Cone

Feng-Yao Chang*and Huei Chu Weng**

Keywords：gas dynamics, high-speed flow, shock waves, heat transfer, spherical nose, tangent-ogive cone, bluntness ratio, detachment distance.

ABSTRACT

This study conducts a computational fluid dynamics (CFD) simulation to predict the thermal-flow fields and characteristics over a spherically blunted tangent-ogive nose cone at a Mach number of 6. The main objective is to analyze the influence of the bluntness ratio (BR) of the spherically blunted tangent-ogive nose cone on the shock wave, velocity, static pressure, static temperature, and density of the airflow around the nose cone under a fixed base radius, ogive radius, and hypersonic Mach number. The computational results reveal that the BR factor causes a change in shock wave type and shape, an increase in shock detachment distance, and an increase in shock layer thickness, and an enhancement in shock wave strength; furthermore, it makes the airflow static pressure, temperature, and density in the shock layer and on the blunted body surface generally increase, but makes the airflow velocity generally decrease. This study provides useful data for rockets, aircrafts, and reentry vehicles in hypersonic flight, especially the heat distribution of temperature, which involves the material selection and internal temperature control during flying-body design. By adjusting the bluntness ratio, it can be found that the maximum static temperature around the nose cone is 1,812.71 K at BR=0, and reaches 2,453.27 K at BR=1.

INTRODUCTION

When the reentry vehicles, such as space shuttle orbiters and capsules, return to Earth from outer space, the surfaces of these hypersonic flying objects will stand severe aerodynamic heating due to surface friction and the high temperature air behind the strong shock waves. Compared with the reentry vehicle with a slender cone, the reentry vehicle with a blunt cone is designed to generate a stronger shock wave, which can increase the heat in the shock layer, thereby reducing the heat load on the flying object. Relatively speaking, these blunt-cone vehicles will experience a large shock wave drag during their reentry and landing. It is revealed that the thermal-flow fields and characteristics over the airflow around the reentry vehicles will be affected by their geometrical shapes. The aforementioned blunt-cone bodies are of many different types, for example, spherically blunted tangent-ogive nose cone. This kind of spherically blunted tangent-ogive nose cone is usually used for the forepart of a rocket, aircraft, or reentry vehicle. The geometrical factors affecting the thermal-flow fields and characteristics over a spherically blunted tangent-ogive nose cone include the nose cone shape, the fineness ratio, and the bluntness ratio. These geometrical factors shown in the literature are discussed as follows.

To study the influence of bluntness ratio on the shock shape of a flying object, O'Bryant (1956) carried out an experimental investigation. It was found that the shock shape for a spherically blunted nose cone with a low bluntness ratio is governed by the conical rear part of the flying object; on the other hand, the shock shape for a nose cone with a high bluntness ratio is governed by its spherical nose. In addition, it was also discovered that the bow shock detachment distance is varied linearly with the spherical nose radius. Owens (1965) did an experimental investigation on the flow past a spherically blunted nose cone at Mach number from 0.5 to 5 and studied the effect of bluntness on the forebody drag of a flying object. It was observed that at higher Mach numbers, bluntness has a great effect on the forebody drag coefficient; on the other hand, the bluntness effect on the forebody drag coefficient is small at relatively low Mach numbers. Harshavardhan et al. (2014) conducted a computational flow analysis of a hypersonic reentry blunt body to numerically investigate the role of a hypersonic flying object's bluntness in aerodynamic

Paper Received January, 2021. Revised February 2021, Accepted February 2021, Author for Correspondence: Huei Chu Weng.

* *Ph.D. Candidate, Department of Mechanical Engineering, Chung Yuan Christian University, Taoyuan 32023, Taiwan, ROC.*

** *Professor, Department of Mechanical Engineering, Chung Yuan Christian University, Taoyuan 32023, Taiwan, ROC.*

heating. The conclusion was that due to the bluntness of the nose cone, a strong shock wave is generated, reducing aerodynamic heating. Hemateja et al. (2017) used a numerical method to study the effect of nose radius on the drag of a blunt cone in supersonic and hypersonic flows. It was found that the drag of the blunt nose cone increases with the increase in the nose radius. Rajput et al. (2017) numerically studied the ogive radius effect on the drag of a blunted tangent-ogive nose cone. The results showed that with a fixed bluntness ratio, the aerodynamic drag coefficient decreases with increasing ogive radius. Zhong et al. (2019) conducted a numerical investigation on the hypersonic flow past the non-axisymmetric blunt body with an aerodisk, whose nose is an ellipsoid, so as to study the aerodisk effects on drag. It was concluded that the total drag of the non-axisymmetric blunt body decreases first and then increases as the aerodisk size increases. Narayan et al. (2018) numerically studied the influences of different nose shapes on the surface heat flux and drag. It was observed that the heat flux variation with the position along the surface of a spherically blunted nose cone is higher than that along the surface of a parabolic nose cone and that for cases where the fineness ratio is less than 1.2, the spherically blunted nose cone provides minimum drag. When the fineness ratio is greater than 1.2, the parabolic nose cone provides superior drag reduction. Hussein et al. (2019) numerically investigated the aerodynamic heating and temperature predicted for different nose cones of a flying body. It was also found that the heat distribution of temperature for a spherically blunted tangent-ogive nose cone is lower than that for a spherical nose cone about 3% at a Mach number of 5 with zero attack angle. Hu et al. (2017) conducted a numerical investigation on the shock wave detachment distance of near space hypersonic vehicles at the altitude of 25 km to 55 km and studied the influencing factors about the detachment distance. They used the least-squares fitting method to deal with the data of the detachment distance and then built a square polynomial formula, which can estimate the detachment distance through the Mach number, the blunt body radius, and the altitude in the atmosphere. Hornung et al. (2019) conducted a numerical study on the variables related to the dimensionless detachment distance and the drag coefficient, and the flow behavior of hypersonic flow through a spherically blunted cone on the spherical and conical surfaces. In this study, a large amount of data was processed using the hypersonic similarity approach, and two formulas for the dimensionless detachment distance and the drag coefficient with density ratio and cone angle parameter were deduced. By means of theoretical analysis, Raghav and Kumar (2015) conducted a similar study and concluded that aerodynamic heating is inversely proportional to the radius of the nose cone.

With reference to the above literature, the study on thermal flow past a blunt nose cone mainly focuses on the shock detachment distance, shock shape, drag, and/or aerodynamic heating of a spherical nose cone, but rarely involves a tangent-ogive nose cone. Regarding the computational fluid dynamics (CFD) simulation for spherically blunted tangent-ogive nose cone, the related literature only focused on the effect of the ogive radius on the external flow fields and characteristics under a fixed bluntness ratio at supersonic speeds and on the comparison between different nose cones for the external thermal fields and characteristics at a Mach number of 5. Moreover, a shock wave is a propagating singular surface across which the static pressure, temperature, and density increase whereas the velocity decreases almost instantaneously. Therefore, in addition to understanding how the bluntness ratio of the spherically blunted tangent-ogive nose cone affects the shock wave type, detachment distance, and strength, it is important to understand exactly how it affects the distributions of the airflow velocity, static pressure, static temperature, and density in the shock layer and on the blunt body surface using CFD.

NUMERICAL SETTING

In this study, ANSYS Fluent software was used in the CFD simulation analysis of the hypersonic thermal flow past a spherically blunted tangent-ogive nose cone. In the numerical setting process, the geometric model was defined first, and then the structured mesh was created, the boundary conditions were set, the CFD solver was employed, the viscosity-temperature relation was determined, and finally the simulation operation was performed, so as to obtain the numerical results. The numerical setting process of simulation analysis is as follows.

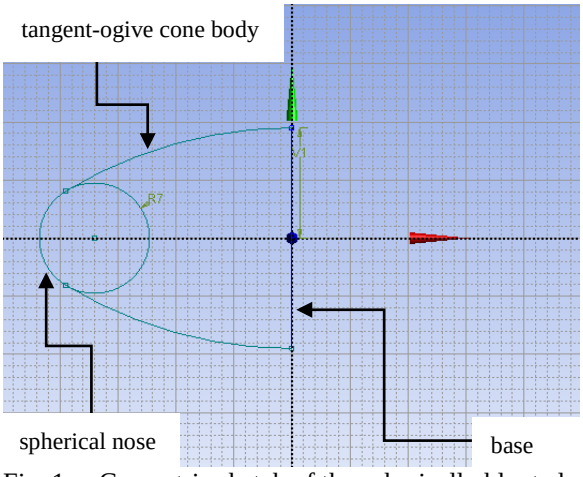

Fig. 1. Geometric sketch of the spherically blunted tangent-ogive nose cone.

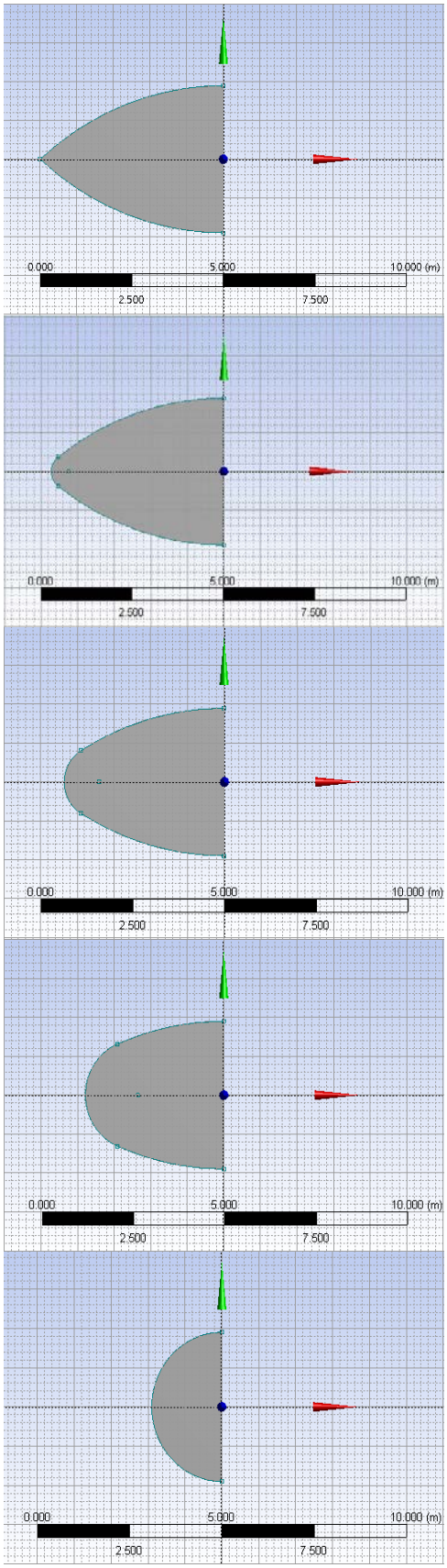

Fig. 2. Cone geometry used in calculations: (a) BR=0.00; (b) BR=0.25; (c) BR=0.50; (d) BR=0.75; (e) BR=1.00.

Geometric Model

A typical two-dimensional (2D) spherically blunted tangent-ogive nose cone used in this study is shown in Fig. 1. It can be divided into three parts: the spherical nose, the tangent-ogive cone, and the base. In order to simplify the analysis, the base diameter and ogive radius of the spherically blunted tangent-ogive nose cone remain fixed and follow the blunt body dimensions of Harshavardhan et al., which are 3.8 m and 7.529 m, respectively. The bluntness ratio BR is defined as the ratio of radius of the spherical nose to the base radius. The BR used in the analysis process has values of 0, 0.25, 0.5, 0.75 and 1, as shown in Fig. 2. It should be noted that due to the nature of the spherically blunted tangent-ogive nose cone, the length from the bottom of the nose cone to the top of the nose cone varies with the BR. The geometric model is a fully tangent-ogive nose cone as BR=0, the geometric model is a spherically tangent-ogive nose cone when the value of BR is greater than 0 and less than 1, and the geometric model is a hemispherical nose cone as BR=1.

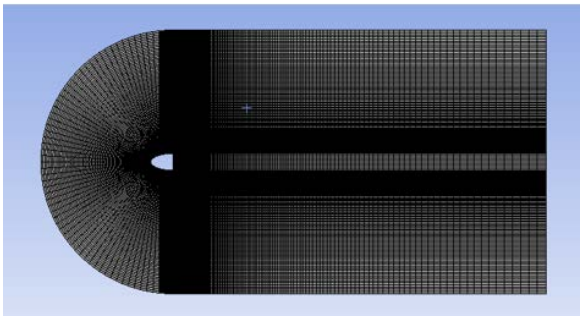

Fig. 3. Structured mesh over the geometry and the domain.

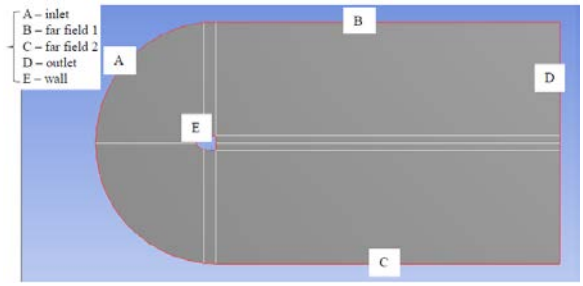

Fig. 4. Boundary condition settings.

Structured Mesh

To obtain high-accuracy calculation results, a structured mesh was employed in this thermal-flow study, as shown in Fig. 3. The thermal-flow field near the nose cone is a relatively important region. Therefore, the mesh near the nose and cone body was made finer by smooth transition. The total number nodes and elements used in this study are 62,690 and 62,200, respectively. The average skewness and average orthogonal quality are 1.5931e-002 and

0.99837, respectively. These statistics reveal that the mesh of this study is maintained in high quality. In addition, the size of the domain used in this study is 15 times the geometric size.

Table 1. Input values in the pressure far field.

Temperature (K)	Static pressure (Pa)	Density (kg/m^3)	Velocity (Mach number)	Viscosity (kg/m·s)
300	0	1.176674	6	1.7894×10^{-5}

Boundary Conditions

Figure 4 shows the boundary condition settings for this study. 'inlet', 'far field 1', 'far field 2', and 'outlet' were set as the pressure far field conditions, and 'wall' was set as the wall condition due to no velocity-slip and temperature-jump conditions on the nose cone surface. The input values in the pressure far field, such as temperature, static (gauge) pressure, density, Mach number, and viscosity, are shown in Table 1.

Governing Equations and Numerical Operation

The numerical operation in this study is a 2D steady-state simulation. Its mathematical models consist of some 2D steady governing equations of motion, written as follows.

Continuity Equation:

$$\frac{\partial(\rho u)}{\partial x}+\frac{\partial(\rho v)}{\partial y}=0 \tag{1}$$

Momentum Conservation Equations:

$$u\frac{\partial u}{\partial x}+v\frac{\partial u}{\partial y}+\frac{1}{\rho}[\frac{\partial p}{\partial x}-\frac{\partial \tau_{xx}}{\partial x}-\frac{\partial \tau_{yx}}{\partial y}]=0 \tag{2}$$

$$u\frac{\partial v}{\partial x}+v\frac{\partial v}{\partial y}+\frac{1}{\rho}[\frac{\partial p}{\partial y}-\frac{\partial \tau_{xy}}{\partial x}-\frac{\partial \tau_{yy}}{\partial y}]=0 \tag{3}$$

Energy Conservation Equation:

$$u\frac{\partial\rho(e+\frac{V^2}{2})}{\partial x}+v\frac{\partial\rho(e+\frac{V^2}{2})}{\partial y}+\frac{\partial(pu)}{\partial x}+\frac{\partial(pv)}{\partial y}=\frac{\partial}{\partial x}(k\frac{\partial T}{\partial x})+\frac{\partial}{\partial y}(k\frac{\partial T}{\partial y})+\frac{\partial(u\tau_{xx})}{\partial x}+\frac{\partial(u\tau_{yx})}{\partial y}+\frac{\partial(v\tau_{xy})}{\partial x}+\frac{\partial(v\tau_{yy})}{\partial y} \tag{4}$$

Here, τ_{yx} and τ_{xy} are the shear stresses lying on the planes normal to the y-axis and x-axis, respectively, τ_{xx} and τ_{yy} are the normal stresses in the x and y directions, respectively, u and v are the velocity components in the x and y directions, respectively, e is the internal energy, p is the pressure, T is the temperature, V is the average fluid velocity, ρ is the fluid density, and k is the fluid thermal conductivity.

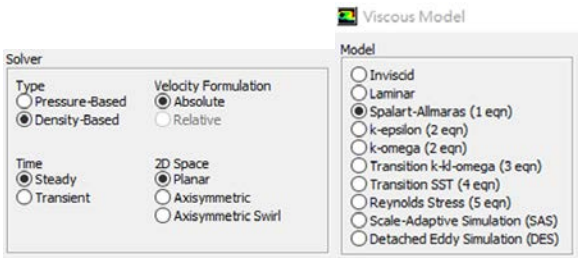

Fig. 5. Simulation model settings.

The gas dynamic mass, momentum, and energy conservation equations (1) to (4) were selected as the governing equations and solved with the viscous model–Spalart-Allmaras model (SA model) for turbulence simulation. The SA model is a relatively simple one-equation model designed for solving the problem on the kinematic eddy (turbulent) viscosity. This model is suitable for the calculation of external flow and turbulent boundary layer flow related to aerospace, especially for the calculation of external flow field around the aircraft with relatively simple geometry, and is applicable to the case where turbulence has little influence on the flow field and the mesh is rough (Spalart and Allmaras, 1992). This model has also been implemented to use wall functions when the mesh resolution is not fine enough (Raghav and Kumar, 2015). Therefore, applying the SA model to this study is a relatively simple and economical calculation method for turbulence simulation. In addition, to solve the problem of compressible and supersonic airflow, the density-based solver was employed, the working fluid, air, was assumed to be an ideal gas ($p=\rho RT$, R is the gas constant), and its viscosity was assumed to be governed by Sutherland's law because this law is sufficient in a wide temperature range and is suitable for the calculation of hypersonic viscous flow (Anderson, 2006). The simulation model settings mentioned above are shown in Fig. 5.

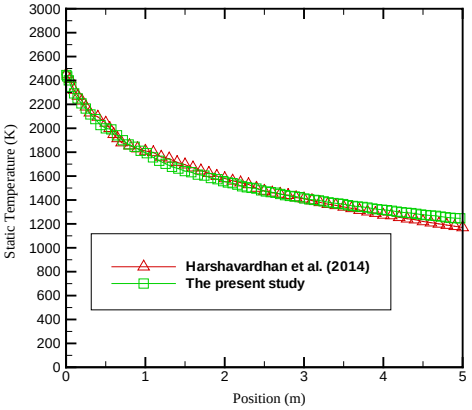

Fig. 6. Comparison of the present results with those reported in literature.

RESULTS AND DISCUSSION

The numerical results shown in this section were obtained through CFD calculations under the conditions of a fixed base radius, ogive radius, and hypersonic Mach number. According to these results, a validation was done and an analysis was carried out as follows.

Numerical Validation

To verify the validation of the present numerical calculation used in this study, a blunt cone, whose shape and size are the same as those used by Harshavardhan *et al.*, was used in the pressure far field set in the literature. Harshavardhan et al. (2014) conducted a CFD simulation to predict the thermal-flow fields and characteristics over a reentry blunt body at a Mach number of 6. However, the shape and size of the blunt body are fixed and not completely a spherically blunted tangent-ogive nose cone (mainly determined by the three geometric parameters: base radius, ogive radius, and nose radius). Therefore, compared with Harshavardhan et al., it can be known in advance whether aerodynamic heating is reasonable if the cone is blunt. Figure 6 presents a comparison between the present numerical results of the static temperature variation with the position along the surface of the nose cone and Harshavardhan *et al.*'s numerical results. It can be seen that our results are in good agreement with those reported in literature (the maximum percentage difference is approximately 6.5%). Note that four sets of grids with different cell numbers (35,200, 47,200, 62,200, and 89,200) and Courant numbers (0.4, 0.6, 0.8, and 1) have been tested, and a cell number of 62,200 and a Courant number of 1 (used in this study) has been shown to be enough to ensure that the numerical solutions are independent. After the numerical validation, the effects of BR on shock wave, airflow velocity, static pressure, static temperature, and density can be further investigated.

BR Effect on Shock Wave

The thin shock layer is one of the characteristics of hypersonic flow. When the Mach number of flow becomes larger and larger, the shock wave will get closer and closer to the surface of the nose cone, making the shock layer thinner and thinner. Therefore, a thinner shock layer will be formed as the flow goes from supersonic to hypersonic through a nose cone. Figure 7 shows the relationship between the shock wave and the bluntness ratio (BR) of the spherically blunted tangent-ogive nose cone. According to the CFD calculation results, as shown in Fig. 7(a), when the bluntness ratio is equal to 0 (BR=0), the shock wave is attached to the fully tangent-ogive nose cone,

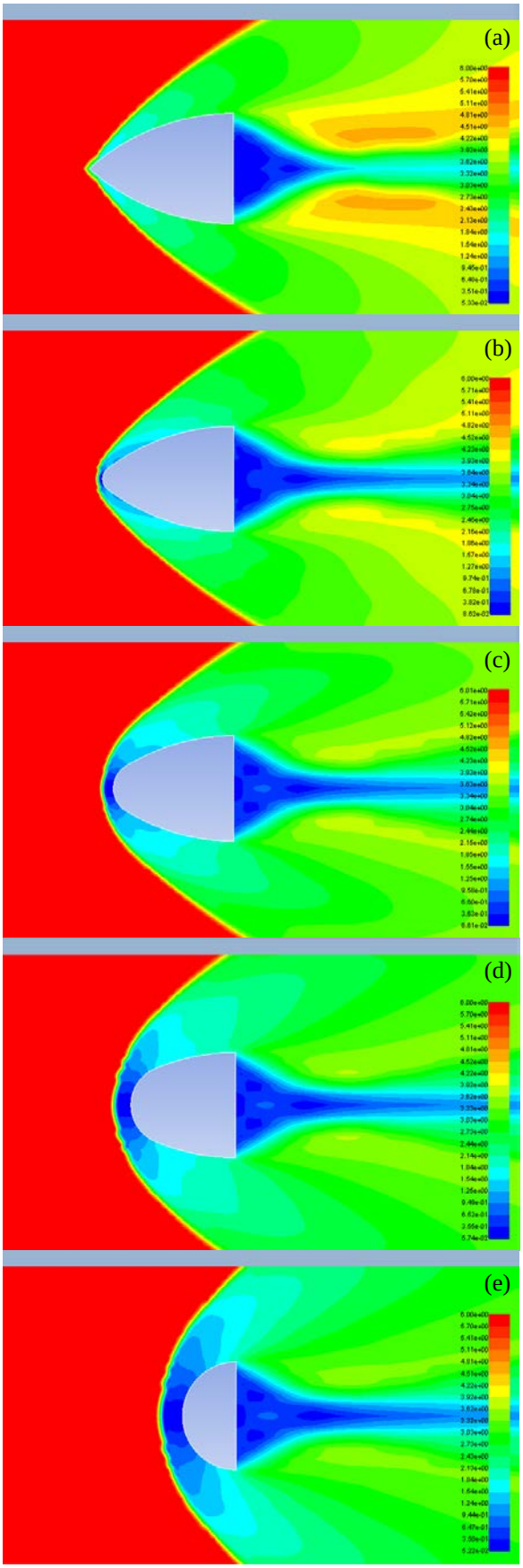

Fig. 7. Mach number contour: (a) BR=0.00; (b) BR=0.25; (c) BR=0.50; (d) BR=0.75; (e) BR=1.00.

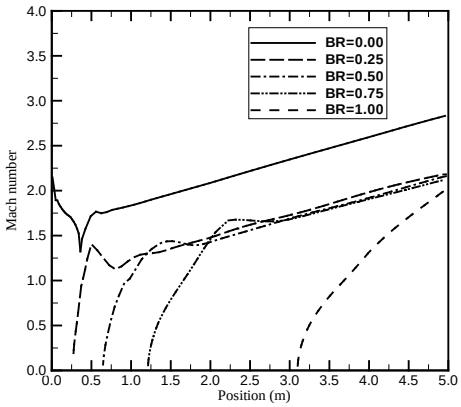

Fig. 8. Velocity distribution over the nose cone for different values of BR.

the so-called attached shock wave. When the value of BR is greater than 0, the shock detachment distance increases with the increase in BR, as shown in Figs. 7(b) to 8, which is similar to the phenomenon found in the experimental study conducted by Machell (1956) at a Mach number of 5.8. Figure 7(b) shows that when the bluntness ratio is slightly greater than 0 (BR=0.25), the bow shock wave is still close to the nose of the spherically tangent-ogive nose cone, but the shock wave and the nose are separated. As shown in Figs. 7(c) to (e), when the bluntness ratio is greater than 0.25 (BR=0.5 to 1), the shock waves around these blunt cones are clearly detach from the noses, becoming detached shock waves. Meanwhile, as BR becomes larger, the shock layer becomes thicker. Moreover, from Figs. 7(b) to (e), it is also found that as BR increases, the wave angle in front of the blunt cone becomes more normal, so the strength of the shock wave becomes stronger. Therefore, we conclude that as BR increases, the type and shape of the shock wave around the nose cone will be changed, the shock detachment distance will be increased, the shock layer will become thicker, and the strength of the shock wave will become stronger.

BR Effect on Airflow Velocity

Figure 7 shows the relationship between the airflow velocity around the nose cone and the BR. From the CFD simulation, it can be found that the velocity of the airflow behind the shock wave is greatly reduced since the airflow is compressed by the shock wave. When BR=0, the shock wave is curved and weak. At this time, the velocity of the airflow behind the shock wave is drastically reduced, but it is still dominated by supersonic flow; that is, the airflow velocity is still above the speed of sound, as shown in Figs. 7 and 8. This means that the stagnation point effect at the center of the fully tangent-ogive nose cone is not obvious. As the value of BR increases, the shape of the nose cone becomes blunter at this time, causing the shock wave angle to become more normal and the shock wave strength to become stronger. In this case, the airflow through the shock wave will be greatly slowed down. On Figs. 7(b) to (e), the blue region represents the region where the airflow velocity is below a Mach number of 0.7. It can be found that as the BR value increases, the blue region becomes larger. In fact, it can also be seen from Fig. 8 that the velocity variation with the position along the surface of the nose cone generally decreases as the BR value increases. Figure 8 shows that the airflow velocity distribution pattern can be changed according to the geometric model. When the geometric model has a tangent-ogive cone, the velocity shows a nearly linear increase with position along the surface of the cone; when the geometric model has a spherical nose, the velocity increases gently with the position along the surface of the nose. Therefore, a nearly linear variation can be observed in the case of BR=0, a non-linear variation can be observed in the case of BR=1, and a combined variation can be observed in other cases (BR=0.25, BR=0.5, and BR=0.75). It is interesting to note that for the case of BR=0, due to the oblique shock wave, the Mach number drops sharply and reaches a minimum at the position 0.26 m, and due to the expansion fan, the Mach number then increases along the nose cone; for the case of BR=0.25, the junction of the spherical nose and the tangent-ogive cone has a significant geometric change, so as the position increases, the velocity suddenly decreases at the junction and then increases as in other cases, which is similar to the conclusion made by Machell (1956) on experimental data with a Mach number of 5.8.

BR Effect on Static Pressure

Figure 9 shows the relationship between the airflow static pressure around the nose cone and the BR. The red regions on these figures indicate the extremely high static pressure regions, which is about 4.00E+06 Pa to 5.59E+06 Pa. From the CFD simulation, it can be found that the static pressure of the airflow behind the shock wave increases drastically because of the compression from the shock wave. When BR=0, the static pressure of the airflow at the center of the fully tangent-ogive nose cone is maintained at about 5.0E+05 Pa. As shown in Figs. 9(a) and 10, the airflows static pressure increases first along the surface of the nose cone and reaches a maximum value of 4.6E+06 Pa at about one-fourteenth of the nose cone length due to the effect of ogive curvature. Then, it rapidly decreases along the surface of the nose cone and tends to be gentle. When the value of BR is greater than 0, the static pressure of the airflow around the surface of the nose cone reaches a maximum at the center of the nose cone, which is about 4.6E+06 Pa, and then

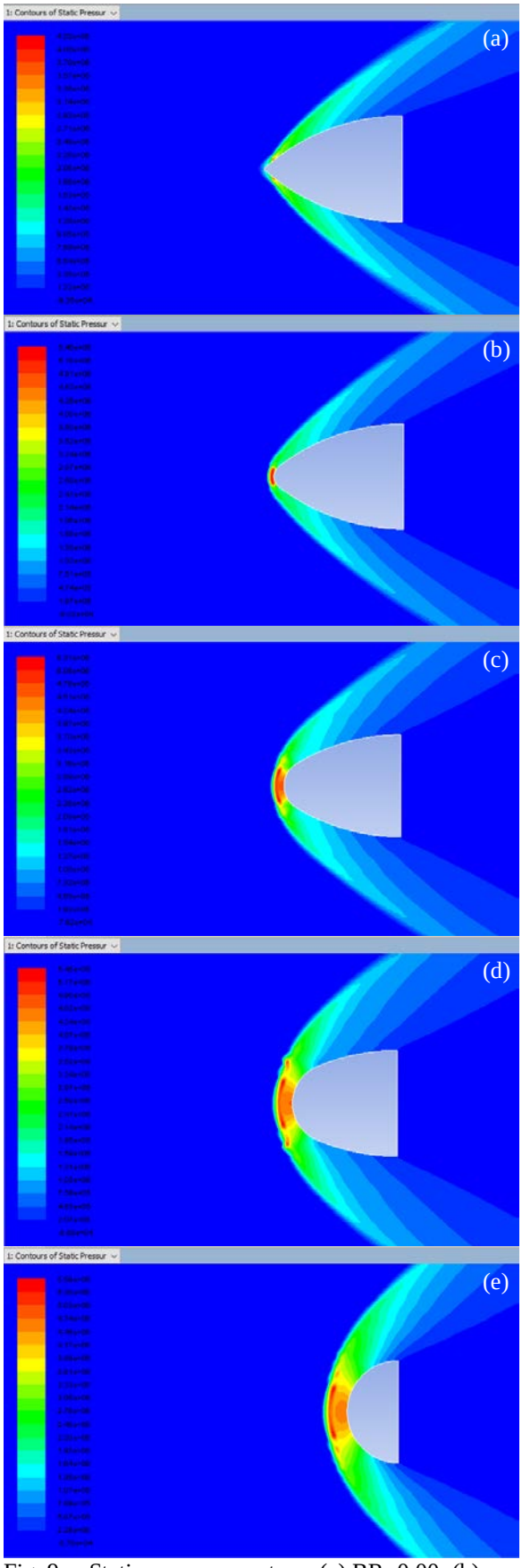

Fig. 9. Static pressure contour: (a) BR=0.00; (b) BR=0.25; (c) BR=0.50; (d) BR=0.75; (e) BR=1.00.

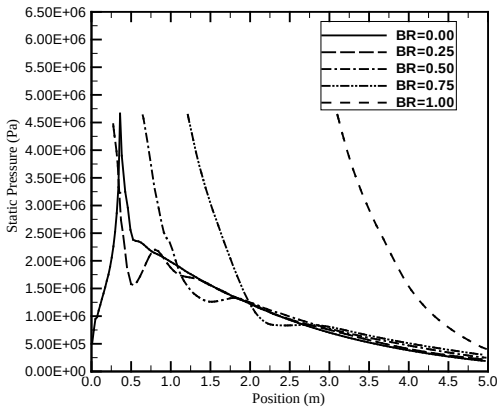

Fig. 10. Static pressure distribution over the nose cone for different values of BR.

decreases rapidly along the surface of the nose cone, eventually tending to zero, as shown in Figs. 9(b) to 10, and furthermore, for a larger value of BR, the airflow static pressure in the shock layer will become greater. Fig. 10 shows that the airflow static pressure distribution pattern can be changed according to the geometric model, similar to Fig. 9(b). When the geometric model has a tangent-ogive cone, the static pressure could show a nearly linear decrease with position along the surface of the cone (but an ogive curvature effect may cause specific behavior to occur, explained later); when the geometric model has a spherical nose, the static pressure decreases gently with the position along the surface of the nose (a similar phenomenon can be found in the experimental study conducted by Kubota (1957) at a Mach number of 7.7). The exception in the figure is mainly due to the effect of ogive curvature that will cause the static pressure to reach a maximum, which is most obvious in the case of the fully tangent-ogive nose cone (BR=0). It is also interesting to note that for the case of BR=0.25, the junction of the spherical nose and the tangent-ogive cone has a significant geometric change, so as the position increases, the static pressure suddenly increases to a maximum value due to an ogive curvature effect, and then decreases as in other cases.

BR Effect on Static Temperature

Figure 11 shows the relationship between the airflow static temperature around the nose cone and the BR. The red regions on these figures indicate the extremely high static temperature regions, which is about 2,200 K to 2,500 K. It can be found from the CFD simulation that due to the conversion of kinetic energy into thermal energy, the static temperature of the airflow behind the shock wave increases drastically. As the BR value increases, the red region becomes larger. In fact, it can also be seen from

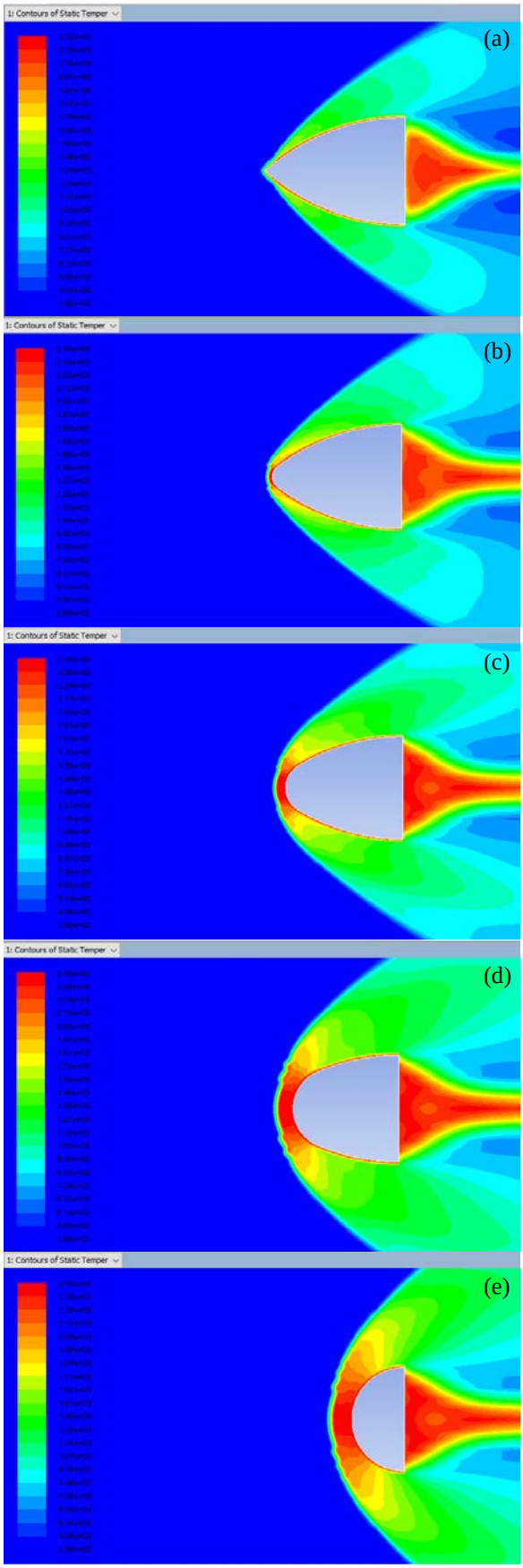

Fig. 11. Static temperature contour: (a) BR=0.00; (b) BR=0.25; (c) BR=0.50; (d) BR=0.75; (e) BR=1.00.

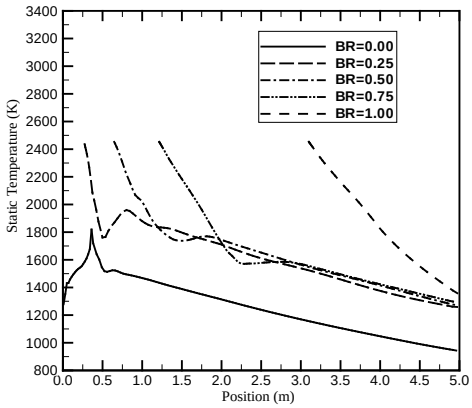

Fig. 12. Static temperature distribution over the nose cone for different values of BR.

Fig. 12 that the static temperature variation with the position along the surface of the nose cone generally increases as the BR value increases. Figure 12 shows that the airflow static temperature distribution pattern can be changed according to the geometric model, similar to Fig. 8. When the geometric model has a tangent-ogive cone, the static temperature shows a nearly linear decrease with position along the surface of the cone; when the geometric model has a spherical nose, the static temperature decreases gently with the position along the surface of the nose. Therefore, a nearly linear variation can be observed in the case of BR=0, a slight non-linear variation can be observed in the case of BR=1, and a combined variation can be observed in other cases (BR=0.25, BR=0.5, and BR=0.75). As interesting as the static pressure distribution is, the junction of the spherical nose and the tangent-ogive cone has a significant geometric change for the case of BR=0.25, so as the position increases, the static temperature suddenly increases to a maximum value due to an ogive curvature effect, and then decreases as in other cases.

BR Effect on Density

Figure 13 shows the relationship between the airflow density around the nose cone and the BR. The red regions on these figures represent relatively high density regions, which is about 6.13kg/m^3 to 8.52 kg/m^3. It can be found from the CFD simulation that due to the compression from the shock wave, the airflow density behind the shock wave increases drastically. When BR=0, the density at the center of the fully tangent-ogive nose cone is maintained at about 1.7 kg/m^3. As shown in Figs. 13 and 14, the density increases first along the surface of the nose cone and reaches a maximum value of 9.1 kg/m^3 at about one-fourteenth of the nose cone length due to the effect of ogive curvature, and then it rapidly decreases along the surface of the nose cone and

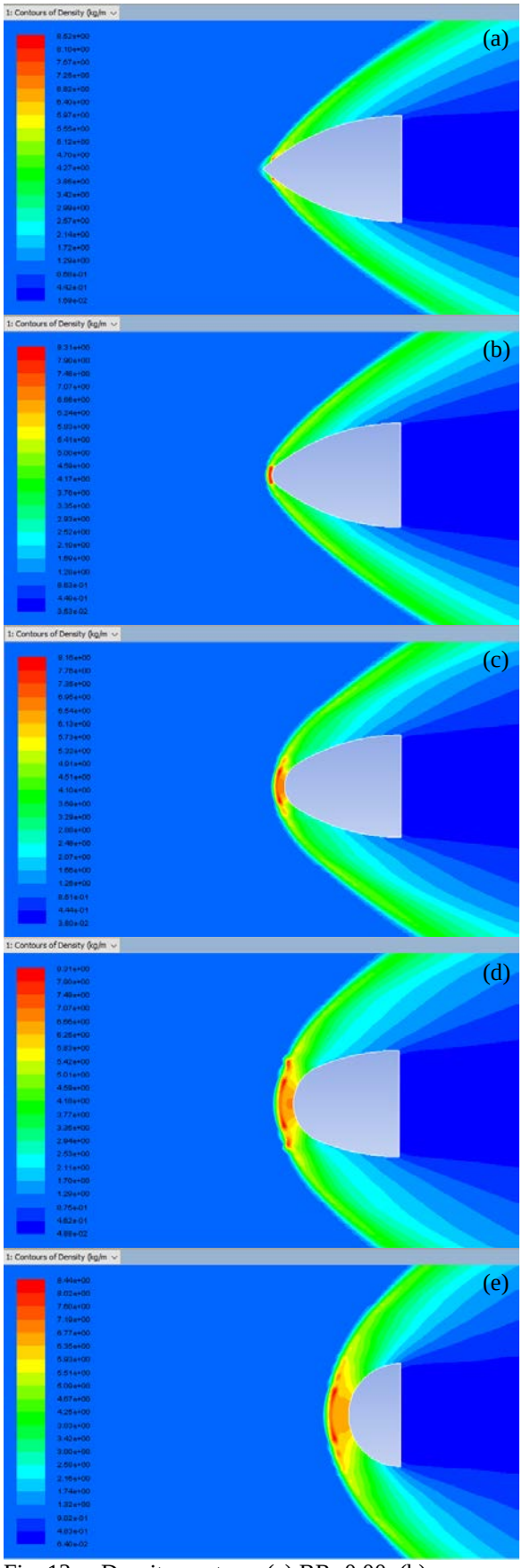

Fig. 13. Density contour: (a) BR=0.00; (b) BR=0.25; (c) BR=0.50; (d) BR=0.75; (e) BR=1.00.

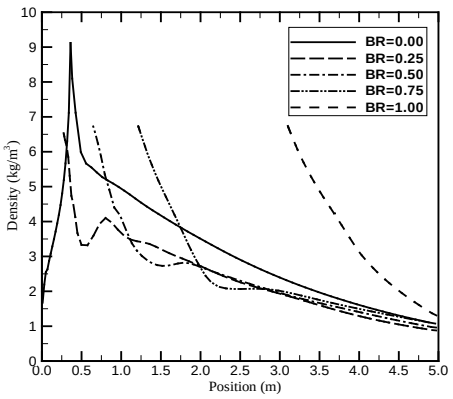

Fig. 14. Density distribution over the nose cone for different values of BR.

tends to be gentle. When the BR value is greater than 0, the maximum density around the nose cone, about 6.52 kg/m^3 to 6.73 kg/m^3, occurs in front of the blunt cone, and then decreases rapidly along the surface of the nose cone, eventually tending to zero, as shown in Figs. 13(b) to 14, and furthermore, for a larger value of BR, the airflow density in the shock layer will become greater. Figure 14 shows that the airflow density distribution pattern can be changed according to the geometric model. This conclusion is similar to the static pressure distribution shown in Fig. 10. It can therefore be concluded that when the geometric model has a spherical nose, the density decreases gently with the position along the surface of the nose; when the geometric model has a tangent-ogive cone, the density, in general, shows a nearly linear decrease with position along the surface of the cone; however, the ogive curvature may cause a local increase in static pressure, resulting in an increase in density with a maximum value. For example, in the case of BR=0, there is a maximum value of density at the position of about 0.36 m, and in the case of BR=0.25, the maximum value of density falls at the position of about 0.8 m.

CONCLUSIONS

The thermal flow past a spherically blunted tangent-ogive nose cone at a Mach number of 6 has been investigated in this study, so as to numerically analyze the influence of the bluntness ratio (BR) of the nose cone on the shock wave, velocity, static pressure, static temperature, and density of the airflow by using ANSYS Fluent software. Through comprehensive analysis, the main results obtained are summarized as follows.

1. As BR increases, the type and shape of the shock wave around the nose cone will be changed, the shock detachment distance will be increased, the shock layer will become thicker, and the strength

of the shock wave will become stronger.

2. The BR factor causes an increase in static pressure, static temperature, and density in the shock layer, but leads to a decrease in velocity. Furthermore, as BR increases, the static pressure, static temperature, and density distributions over the nose cone generally increase, but the velocity distribution generally decreases.

This study may benefit the investigations of the rockets, aircrafts, and reentry vehicles, such as space shuttle orbiters and capsules.

ACKNOWLEDGMENT

This work was financially supported by the Ministry of Science and Technology of Taiwan under Grant No. MOST 108-3116-F-042A-006.

REFERENCES

Anderson, J.D, *Hypersonic and High Temperature Gas Dynamic*, McGraw-Hill (2006).

Harshavardhana, N.S., Sanjana, K., Sai Sharan, K., and Srinivas, G., "Computational Flow Analysis of Hypersonic Reentry Blunt Body using Fluent and Gambit," *Int. J. Sci. Eng. Technol. Res.*, Vol.5, pp.262-269 (2014).

Hemateja, A., Ravi Teja, B., Dileep Kumar, A., and Rakesh, S.G., "Influence of Nose Radius of Blunt Cones on Drag in Supersonic and Hypersonic Flows," *IOP Conf. Ser.: Mater. Sci. Eng.*, Vol.225, p. 012045 (2017).

Hornung, H.G., Schramm, J.M., and Hannemann, K., "Hypersonic Flow Over Spherically Blunted Cone Capsules for Atmospheric Entry. Part1. The Sharp Cone and the Sphere," *J. Fluid Mech.*, Vol.871, pp. 1097-1116 (2019).

Hu, Y.M., Huang, H.M., and Guo, J., "Shock Wave Standoff Distance of Near Space Hypersonic Vehicles," *Sci. China Technol. Sci.*, Vol.60, pp. 1123-1131 (2017).

Hussein, E.Q., Rashid, F.L., and Azziz, H.N., "Aerodynamic Heating Distribution for Temperature Prediction of Fast Flying Body Nose using CFD," *J. Adv. Res. Fluid Mech. Therm. Sci.*, Vol.64, pp.183-195 (2019).

Kubota, T. *Investigation of Flow Around Simple Bodies in Hypersonic Flow*, Ph.D. Dissertation, California Institute of Technology (1957).

Machell, R. M., *An Experimental Investigation of Hypersonic Flow over Blunt Nosed Cones at a Mach Number of 5.8*, Engineer's Thesis, California Institute of Technology (1956).

Narayan, A., Narayanan, S., and Kumar, R., "Hypersonic Flow Past Nose Cones of Different Geometries: A Comparative Study," *Simul.-T. Soc. Mod. Sim.*, Vol.94, pp.665-680 (2018).

O'Bryant, W.T., *An Experimental Investigation of Hypersonic Flow over Blunt Nosed Cones at a Mach number of 5.8*, Engineer's Thesis, California Institute of Technology (1956).

Owens, R.V., "Aerodynamic Characteristics of Spherically Blunted Cones at Mach Number from 0.5 to 5.0," Technical note, NASA TN D-3088 (1965).

Raghav, P.H. and Kumar, G.D., "Flow Analysis on Various Bluff Bodies," *Int. J. Innovative Sci. Eng. Technol.*, Vol.2, pp.579-600 (2015).

Rajput, B., Pandey, P.K., Narayan, A., and Narayanan, S., "Computational Study of Supersonic Flow Past Blunted Tangent-Ogive Nose Cone," *Int. J. Adv. Res. Sci. Eng.*, Vol.6, pp.818-824 (2017).

Spalart, P.R. and Allmaras, S.R., *A One-equation Turbulence Model for Aerodynamic Flows*, American Institute of Aeronautics and Astronautics 92-0439 (1992).

Zhong, K., Yan, C., Chen, S.S., Zhang, T.X., and Lou, S., "Aerodisk Effects on Drag Reduction for Hypersonic Blunt Body with an Ellipsoid Nose," *Aerosp. Sci. Technol.*, Vol.86, pp.599-612 (2019).

極音速球狀切面尖拱形鼻錐之熱流分析

張峰垚　　翁輝竹
中原大學機械工程學系

摘 要

本研究進行了計算流體動力學（CFD）模擬，以預測馬赫數為 6 的球狀切面尖拱形鼻錐之熱流場及特性。主要目的是分析在固定的基本半徑、尖拱半徑及極音速馬赫數下，鈍度比（BR）對球狀切面尖拱形鼻錐周圍沖擊波、速度、靜壓力、靜溫度及密度之影響。計算結果顯示，BR 因子會引起衝擊波類型和形狀的變化、衝擊脫離距離的增加、衝擊層厚度的增加，以及沖擊波強度的提高。此外，一般而言，BR 因子使得衝擊層中和鈍體表面上的氣流靜壓力、靜溫度及密度增加，但使得氣流速度降低。研究結果為極音速飛行中的火箭、飛機及再入飛行器提供了有用的數據，尤其是溫度的熱分佈，這涉及飛行物體設計過程中的材料選擇和內部溫度控制。通過調整鈍度比，本研究可發現鼻錐周圍的最大靜溫度在 BR=0 時為 1,812.71 K，在 BR=1 時達到 2,453.27 K。